Acta Cryst. (1995). D**51**, 914–924

Refinement of Purothionins Reveals Solute Particles Important for Lattice Formation and Toxicity. Part 2: Structure of β-Purothionin at 1.7 Å Resolution

BY BOGUSLAW STEC, USHA RAO AND MARTHA M. TEETER*

Department of Chemistry, Boston College, Chestnut Hill, MA 02167, *USA*

(*Received* 29 *June* 1994; *accepted* 1 *March* 1995)

Abstract

The crystal structure of β-purothionin (β-PT) has been determined at 1.7 Å resolution. β-PT and previously solved α_1-PT belong to a family of membrane-active plant toxins homologous to crambin. β-PT crystallizes in the same space group as α_1-PT (*I*422) but with the *c* axis 3 Å longer than α_1-PT. The unit-cell dimensions of β-PT crystals are $a = b = 53.94$ and $c = 72.75$ Å. Two data sets were collected on a multiwire area detector, each with R_{sym} around 6.0%, and were merged to get a single data set at 1.7 Å ($R_{merge} = 9.6\%$). The X-ray structure of α_1-PT was used to build a starting model for β-PT. The β-PT model was refined using the program *PROLSQ* from 10 to 1.7 Å resolution to an *R* factor of 19.8% with very good geometry. The final structure contains 439 atoms including 337 protein atoms, 77 waters, two acetates, two glycerols and one phosphate. The high-resolution structure of the β-PT agreed well with that of the lower resolution α_1-PT structure only after the latter was extensively rerefined. Both refinements revealed phosphate and glycerol molecules which are important in lattice formation. The binding of phosphate and glycerol molecules to purothionins (PT) was confirmed by NMR and was implicated in the biological activity of toxins. Modeling of phospholipid binding to PT based on glycerol and phosphate-binding site could shed light on the lytic toxicity of this protein-toxin family. Although the structures of α_1-PT and β-PT preserve the overall fold of crambin, they exhibit key differences that are directly relevant to the toxicity of thionins.

1. Introduction

Thionins constitute an important family of plant toxins (Bohlman & Apel, 1991) which are ~60% homologous to crambin. The crystal structure of a member of this family, α_1-purothionin (α_1-PT), has recently been determined in our laboratory at 2.5 Å resolution (Teeter, Ma, Rao & Whitlow, 1990; Rao, Stec & Teeter, 1995). Because of inherent problems with the α_1-PT crystals, however, higher resolution data could not be collected from these crystals. In order to better understand the toxic behavior of these thionins (Carrasco *et al.*, 1981), we crystallized β-purothionin (β-PT) and obtained well ordered crystals. After several modifications to initial crystallization conditions, crystals diffracting to 1.7 Å were obtained.

β-PT has about 88% sequence identity with α_1-PT. It differs from α_1-PT only at five residues out of 45 residues. The important changes are at positions 27 and 42 where glycine residues are replaced by asparagine and aspartic acid, respectively (Fig. 1). These changes should not induce major changes in the backbone structure. The structure of β-PT should, therefore, be very similar to that of α_1-PT. With this knowledge, a crystallographic study of β-PT was undertaken in order to (i) ascertain the structural similarities between the two purothionins and (ii) determine the structure at higher resolution so as to understand the toxic behavior in greater detail. We used homology modeling to build a model of β-PT by replacing those residues of the α_1-PT model which are different in β-PT. The resulting model has been used to solve the X-ray structure.

This paper describes the crystallization of β-PT, its crystal structure determination at 1.7 Å resolution and its comparison to the α_1-PT structure. The sequence differences between crambin and these thionins contribute directly to the membrane activity of the toxins.

2. Experimental procedures

2.1. *Crystallization of β-PT*

2.1.1. *Crystallization conditions.* Plate-like crystals of β-PT were grown by sitting-drop vapor-diffusion methods similar to those used for growing crystals of α_1-PT (Teeter *et al.*, 1990). As precipitant we used either 2-methyl-2,4-pentanediol (MPD) or *sec*-butanol. A typical crystallization with *sec*-butanol consisted of a 20 ml dip with 50 mg ml^{-1} β-PT in sodium cacodylate (CAC) buffer at pH 5.9 to which 8 to 15%(*v*/*v*) *sec*-butanol was added. The dip was equilibrated against 12% *sec*-butanol and 17% $MgCl_2$ in 90 m*M* CAC buffer (pH = 5.9) at room temperature. Plate-like crystals were readily obtained in a week.

In the case of MPD as precipitant, crystals were obtained when dips containing 10 or 15% MPD were equilibrated against 10% MPD and 22% $MgCl_2$ in the reservoir. Slightly thicker crystals were obtained when the dips contained a trace amount (1.0%) of dioxane. Most of the crystals had dimensions of 0.2 × 0.2

* To whom correspondce should be addressed.

× 0.05 mm. We also tried different buffers, and crystals were obtained in *N*-(2-acetamido)-iminoacetic acid (ADA) at pH 6. They were more fragile than crystals obtained from CAC.

The presence of $MgCl_2$ in the reservoir seemed critical in all these set ups. Since *sec*-butanol had a phase separation at 20% concentration, higher concentrations could not be used. Hence, $MgCl_2$ was necessary to drive water out of the dip. The crystals obtained by these methods, however, had an intrinsic tendency for twinning: they looked like thin plates stacked one over the other with a slight rotation between layers.

2.1.2. *Stabilization of the crystals.* Initial attempts were made to collect X-ray diffraction data from the plate-like crystals grown from CAC buffer but several problems were encountered. Crystals were very tiny and dissolved quickly when the crystallization boxes were opened. Since they were grown from alcohol at a very critical equilibrium concentration, they redissolved in the mother liquor even at minimal evaporation of the alcohol. Additional problems were posed by the small amount of mother liquor around the crystals. Various methods of crystal mounting such as oil mounting, glovebox mounting, *etc.* were tried to circumvent these problems in vain. Hence we developed a stabilization procedure for the crystals.

Various concentrations of MPD and $(NH_4)_2SO_4$ (AS) were tried both individually and in combination. 100% of ammonium sulfate (AS) alone caused the crystals to dissolve and reappear as precipitate whereas MPD alone resulted in the development of cracks in the crystals. Finally a mixture of 30% saturated AS and 8% MPD seemed to stabilize the crystals well.

2.1.3. *Improvement of the crystal quality.* Because of the role of AS in stabilizing the crystals, attempts were made to crystallize in the presence of AS as well. Large crystals were grown from 20 ml dip containing 15 mg ml^{-1} β-PT, 2% dioxane, 5% MPD and 58% AS in 75 m*M* CAC buffer (pH = 5.9) equilibrated against 10% MPD and 20% $MgCl_2$ in 90 m*M* CAC buffer. The presence of AS prevented drying of the dips by lowering the solubility of the protein.

A thick large crystal was therefore cut to a size of 0.4 × 0.4 × 0.2 mm, stabilized with the previously described solution, and mounted in a glass capillary. The crystal diffracted well (up to 2.1 Å). The β-PT crystals belong to the same space group ($I422$) as α_1-PT with similar cell parameters: $a = b = 53.94$, $c = 72.75$ Å and $\alpha = \beta = \gamma = 90°$. The c dimension of β-PT was larger than for α-PT by ~3 Å.

Eventually, even better crystals of ~0.5 × 0.3 × 0.2 mm size were grown in about 10 d when a mixture of MPD, polyethylene glycol (PEG) and AS was used as precipitant. Here a 20 ml dip containing 50 mg ml^{-1} of β-PT in 90 m*M* CAC with 10% MPD, 2.5% PEG 4000 and 8% AS was equilibrated against a reservoir containing 10% MPD and 20% $MgCl_2$ in 75 m*M* CAC (pH = 5.9). This batch of crystals diffracted to 1.7 Å resolution.

2.2. *Data collection and analysis*

Two different data sets were collected using a Xuong–Hamlin multiwire area detector powered by a Rigaku RU200 rotating-anode generator at 50 kV and 100 mA equipped with a graphite monochromator. A monochromatized Cu $K\alpha$ X-ray beam was used.

The crystal to detector distance was 400 mm, which along with the detector 2θ value (19°) allowed the data collection to 2.1 Å resolution. Intensity and σ of each observation along with all indexing and background corrections were calculated simultaneously with the scanning process.

In this manner, 11 407 observations of 2646 independent reflections were collected for β-PT. The data was reduced by software provided by San Diego Multiwire Systems, the intensities were next reduced by applying the usual Lorentz and polarization corrections, scaled together in 55 increments of ω, and averaged. Final R_{sym} ($R_{sym} = \Sigma_i|\langle I\rangle - I_i|/\Sigma\langle I\rangle$) for the data was 5.63%. This data set was 99% complete to 2.31 Å and contains 66% data to 2.25 Å. The overall fraction of data measured above 2σ is 97%.

A second native data set has been collected on a fresh crystal grown in the presence of mineral oil. Mineral oil, which was a remnant from our previous oil mounting attempts, was present in the droplets and the crystals formed readily on the interface between oil and mother liquor. The better crystal quality and the use of crystal-to-chamber distance of 400 mm with the 2θ value of the detector being –32° allowed the data to be collected up to 1.7 Å resolution. A total of 44 767 reflections comprising of 4595 unique reflections were measured and reduced as described above with R_{sym} being 6.1%. However, due to interruption in the data-collection procedure, we collected only 80% of the data. Therefore, we merged the

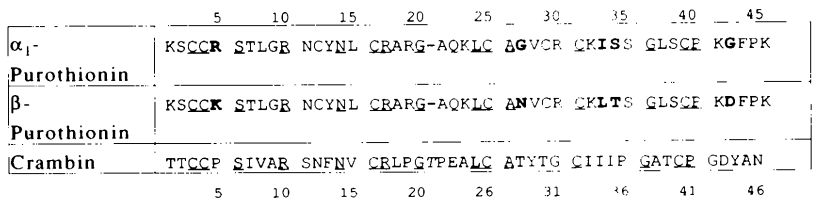

Fig. 1. Sequence alignment of crambin, α_1- and β-purothionin. Substitutions between the forms are in bold and amino acids identical for the family are underlined. Insertion in crambin is in italics.

Table 1. *Summary of various stages of refinement of the β-PT structure*

Stage	Adjustments to the model	Resolution (Å)	Total No. atoms	Total No. waters	No. of others*	No. of cycles	*R* factor (%)
1	α_1-PT model (R = 18.4) with side chains changed to fit β-PT	2.4	337	0	0	26	26.3
2	Side chains of the residues 5, 27, and 42 were corrected	2.4	419	22	1 MPD 1 ACT	35	21.7
3	Side chains of the residues 1, 19, 30, 34 and 38 were corrected, MPD changed to GLC and POS introduced	2.25	439	439	2 GLC 1 ACT 1 POS	35	18.7
4	Side chains of the residues 23 and 32 and GLC were corrected	1.7	464	72	2 GLC 1 ACT 1 POS	30	22.4
5	Another ACT was introduced and GLC corrected	1.7	483	77	2 GLC 2 ACT 1 POS	48	19.8

* Abbreviations used here: MPD, 2-methyl-2,4-pentanediol; GLC, glycerol; ACT, acetate ion; POS, phosphate ion.

two data sets. They were scaled in different resolution ranges and the data from the second set in the 2.3–1.7 Å resolution range were merged with the 2.3 Å data of the first set. The merged data set contained 5092 reflections with an R_{merge} of 9.6%.

2.3. *Modeling and refinement of the βPT structure*

The model for β-PT was constructed from partially rerefined α_1-PT model at 18.4% R value (reduced from 21.6%, Teeter *et al.*, 1990) by changing the appropriate residues in *FRODO*. All these changed residues were subjected to about 30 cycles of Hermans' geometric refinement (1974) using the *FRODO* package. Because of the small number of changes, global energy minimization was not used. However, side chains were placed in their most statistically favored rotamer positions (Ponder & Richards, 1987).

The resulting model with 337 atoms was used as the starting model for the restrained least-squares refinement. All the refinement was carried out using the *PROLSQS* software package of Hendrickson modified by Sheriff (1987) to include van der Waals restraints on symmetry relations. One cycle of refinement required approximately 25 min of central processing unit (c.p.u.) time on a Vaxstation 3500.

The program *PROTINS* was used to impose intermolecular non-bonded contacts. Restraints on distance, non-bonded contacts, chiral volume and planarity were imposed on additional solute molecules such as glycerol, phosphate and acetate during the refinement. Non-bonded restraints were imposed on the water molecules.

Table 1 summarizes the course of the refinement and Table 2 gives the final refinement parameters. Each round of refinement consisted of a session of model building followed by refinement to convergence. Five rounds of refinement were performed. Typical remodeling included side-chain conformation modification and modeling of new solvent sites. Refinement began with the data above 2σ up to 2.4 Å. After the second round, all the data (above 2σ) to 2.25 Å were added.

Table 2. *Summary of restrained least-squares refinement parameters for β-PT*

	Target σ	R.m.s. deviation
Average ΔF		259.22
R factor*		0.198
R_{error}†		0.072
No. of structure factors ($> 2.5\sigma$)		4966
Structure-factor weight‡	220	343.5
R.m.s. deviations from ideal (Å)		
Bond distances	0.02	0.017
Angle distances	0.03	0.031
Plane 1–4 distances	0.04	0.040
R.m.s. deviation from planarity (Å)	0.015	0.008
R.m.s. deviation from ideal chirality (Å^3)	0.15	0.174
R.m.s. deviations from permitted contact distances (Å)		
Single-torsion contacts	0.5	0.169
Multiple-torsion contacts	0.5	0.193
Possible hydrogen bond	0.5	0.207
R.m.s. deviations from ideal torsion angles (°)		
For planar group (0 or 180)	5.0	2.0
For staggered group (60 or 180)	18.0	19.6
For orthogonal group (90)	20.0	1.8
R.m.s. deviations of the isotropic thermal factor differences (Å^2)		
For main-chain bond	2.0	1.45
For main-chain angle	3.0	1.57

* $R = \sum_h ||F_o|| / \sum_h |F_o|$, where h is over all h, k, l.
† $R_{error} = \sum_h |\sigma(F_o)| / \sum_h |F_o|$.
‡ The weight chosen for the structure-factor refinement, the 'target σ' of ΔF, was modeled by the function, $\omega = (1/\sigma)^2$ with $\sigma = 220 + [(-1000.0)(\sin\theta/\lambda - 1/6)]$.

The $F_o - F_c$ map produced after the first 26 cycles of refinement (round 1) showed clearly new conformations for residues 27 and 42 which are different from those of α_1-PT. Asp42 could be fit into the cleft formed by the residues Phe43 and Pro40 in a similar conformation as in crambin. Appropriate changes to these residues along with a minor correction to Lys5 were made during round 2. The side chains of residues such as Arg19, Lys1, Lys32, Lys23 and Lys41 attained new conformations which may be ascribed to the difference in contacts between α_1-PT and β-PT molecules in the crystals. These side chains were modeled during rounds 3 and 4.

2.4. *Solvent/solute modeling*

Criteria used to model the solvent structure evolved during the course of refinement. The initial water model of β-PT was predicted using a template for water around polar groups in proteins derived from the analysis of crystal structures at 1.4 Å or better resolution (Roe & Teeter, 1993). This method can be useful for an initial crystallographic refinement of water as well as for model building in general. Templates for water prediction had been derived from high-resolution structures by superimposing the hydrogen-bonding groups around Arg, Glu, Asp, Asn and Gln. The waters around these residues were added to the structure that had been refined to convergence without water. The *R*-factor dropped by 2% when these water positions were refined and all but two out of 22 waters added were found to be correct. Subsequent water positions were modeled by inspecting the $F_o - F_c$ electron density and if a peak fell within 2.5 to 3.5 Å of an atom of the model that was capable of hydrogen bonding, the peak was accepted as a site for solvent. Only the first shell of the solvent was modeled in the beginning.

As in the case of α_1-PT, large peaks of difference densities were observed on the polar face of the protein. An acetate ion was modeled at the intersection of two twofold axes. In the density close to Tyr13, an MPD* molecule was introduced at first. MPD was used in crystallization and was thought to have the correct shape and number of atoms to fit the density. Unfortunately, after 25 cycles of refinement the tetrahedral group of disubstituted carbon of the MPD molecule was flattened and distorted, and showed imperfect fit to the density. After careful inspection of the densities and possible head groups of phospholipids, a glycerol molecule was modeled at this site and it refined very well (Fig. 2). The electron-density maps with improved phases clearly showed a new conformation for the glycerol as compared with α_1-PT. The O2 atom bound in α_1-PT to the Gln22 formed a hydrogen bond to the NZ of symmetry-related Lys45 in β-PT. The discussion of the possible sources of glycerol was presented in the previous paper (Rao, Stec & Teeter, 1995).

The two positions at which we had detected the *sec*-butanol in α_1-PT were carefully inspected. The density at the hydrophobic face which corresponded to *sec*-butanol in α_1-PT was larger. Thus, we modeled a second glycerol molecule at this site. Since our crystallization solution did not contain *sec*-butanol, the other *sec*-butanol position, close to the N terminus, proved not to be occupied.

The modeling of a phosphate ion was also not entirely straightforward. The shape of the electron density at the location that corresponded to a phosphate ion in α_1-PT was not indicative of a phosphate ion at the beginning. However at stage 3, a phosphate ion was modeled at this site. Introduction of phosphate along with 35 cycles of refinement at round 3 resulted in a final *R* factor of 17.8% at 2.25 Å. Elevated temperature factors for the phosphate ion and weaker electron density as compared to α_1-PT suggests that it is possible that phosphate was partially replaced by sulfate. After addition of all the data to 1.7 Å resolution at stage 4 and 5 and two modeling sessions, the *R* factor refined to the level of 19.8%. At stage 4 side chains of Lys23 and Lys32 were corrected as indicated by the density at 1.7 Å. At stage 5 an additional acetate molecule was added at the charged cluster near Arg30. The final model has a total of 439 atoms including 337 protein atoms, 77 waters, two glycerol molecules, two acetates and one phosphate.

3. Results and discussion

3.1. *Quality of the structure*

The quality of the refined structure can be assessed using various analyses. The *R*—free method (Brünger,

* Solute molecules were constructed in *QUANTA* (Polygen Corporation, 1991).

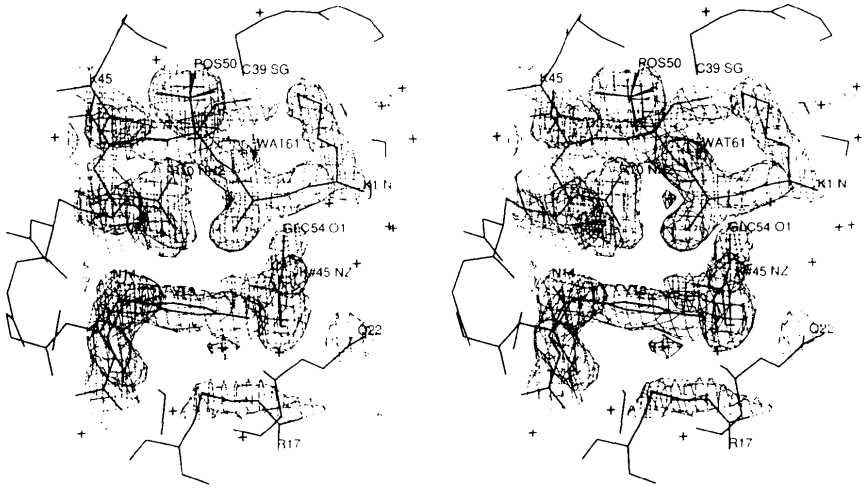

Fig. 2. Stereoview of the of the phosphate–glycerol-binding site in β-PT. Please note conformational changes of Lys1 and the glycerol molecule. The map is contoured at the 1.6σ level.

1992*a*,*b*) showed the decorrelation (difference between the main and the test data sets) in an acceptable range (~10%) with R_{Main} = 19.96% and R_{free} = 28.13%. A Luzzati plot (Luzzati, 1952) shown in Fig. 3 gives a nearly ideal fit of 0.22 Å for positional errors in atomic coordinates.

The r.m.s. deviation in distances from ideal values falls close to or within targeted variances (see Table 2). Only ~5% of all distances in the three categories tabulated in *PROLSQ* fall two standard deviations outside of their ideal values.

The r.m.s. deviation of atoms of planar groups from their fitted planes is 0.008 Å, which is well within the targeted value of 0.015 Å. No planar deviation is beyond two standard deviations of the target variance. The low variance in planar groups reflects, to a large extent, the tight distribution of the ω torsion angle of about 180°. Since a wider ω-angle distribution is found in highly refined structures like crambin (Teeter, Roe, & Heo, 1993) as well as in polypeptides (Ashida, Tsungoae, Tanaka & Yamane, 1991), the restraints were relaxed to 5.0 Å.

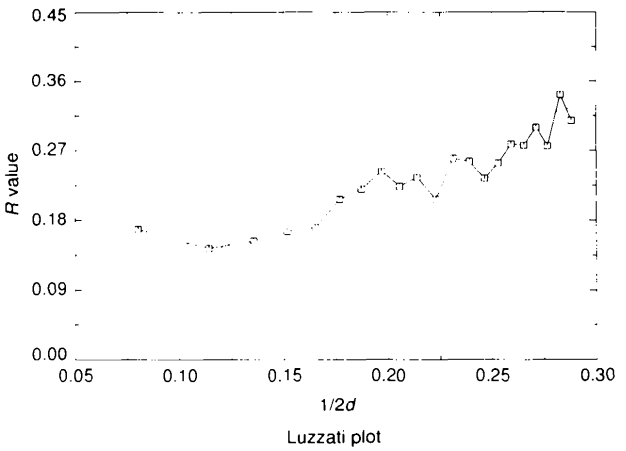

Fig. 3. Luzzati (1952) plot of R factor as a function of resolution ($\sin\theta/\lambda$). The broken lines (Δr = 0.2, 0.25, 0.30) show the theoretical variation in R for non-centric data (10–1.7 Å), when only coordinate errors of the model contribute to the difference between the observed and calculated quantities.

The dihedral angles of the main chain as well as the side chains generally conform well to their expected values. All of the side-chain conformations (χ_1,χ_2) are in allowed regions of Ponder & Richards' library (1987) except four arginines, Arg10, Arg17, Arg19 and Arg30. This deviation of arginines can be explained in terms of crystal contacts or similarities to crambin.

In general, the electron density for the model is excellent (Fig. 4). All of the backbone atoms have uniquely defined positions by the density. Even for the long side chains such as those of arginines, all the atoms, especially atoms in guanidinium groups are clearly visible. Only Arg30 and Lys41 seem to have weaker densities.

Weak negative difference electron density was observed on Asn27 and Asp42. This fact plus relatively high temperature factors for those side chains suggests that these crystals may be a mixed form of α_1- and β-purothionins in the β-lattice. Only those two residues are distinct enough to show the differences in sequence between the two forms. An attempt was made to establish the ratio by refining occupancy of those residues. The final occupancy was ~80% for β-PT

The temperature factor *versus* residue profile (Fig. 5) shows the same type of mobility in both structures and is reminiscent of that for crambin. The temperature factors of β-PT are slightly higher than those of α_1-PT (Fig. 5) as well as those of additional solute molecules. This may be attributed both to the fact that β-PT crystals appear to be a mixture of two forms (see above) and to the looser packing for helix 2 in β-PT lattice. Variation in crystal contacts from crystal to crystal can also explain a relatively high R_{merge} between both data sets.

3.2. *Description of the structure*

The secondary structure of β-PT and overall folding is the same as that of α_1-PT (Teeter *et al.*, 1990; Rao *et al.*, 1995). The α_1- and β-PT structures resemble that of crambin, with the general shape of the Greek capital letter gamma (Γ). The vertical stem (Fig. 6) is comprised of two antiparallel α-helices, and the horizontal arm has a coil in extended conformation and a short

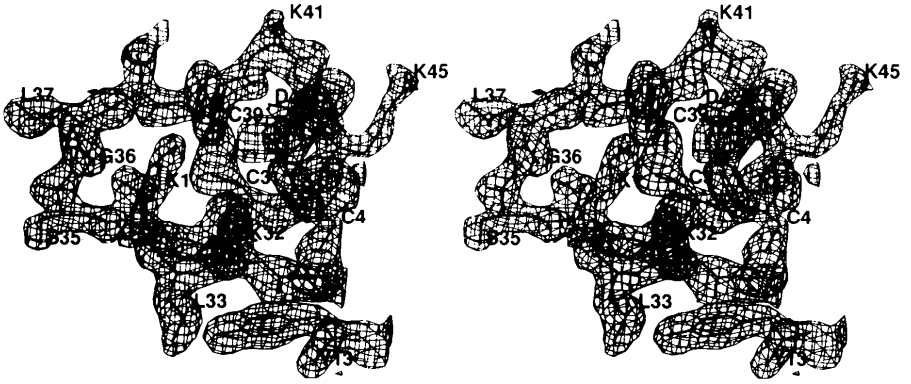

Fig. 4. Stereoscopic view of a typical electron-density map superimposed on the appropriate part of the β-PT model. Residues which make the β-sheet (1–5 and 30–34) are shown. Parts of residues 6, 10, and 43 are also included. The map is contoured at the 1.6σ level.

Table 3. *Intramolecular hydrogen bonds in α_1- and β-PT*

Acceptor	Donor	Distance in β-PT (Å)	Distance in α_1-PT (Å)
Lys23 O	Asn27 OD1	2.92	Not present
Asp42 OD1	Asp42 N	2.85	Not present
Thr34 OG1	Gly36 N	3.04	Not present
Thr34 OG1	Ser35 N	2.98	Not present
Ser34 OG	Ser38 O	Not present	2.91
Thr7 OG1	Thr7 N	2.83	3.12
Thr7 OG1	Leu8 N	2.92	2.84
Ser6 OG	Gly9 N	3.24	2.91
Lys45 OT*	Arg10 NE	2.87	2.62
Lys45 O*	Arg10 NH2	2.92	2.73
Ser2 O*	Arg10 NH2	2.96	2.76
Ser2 OG*	Arg10 NH1	2.92	2.87
Gly20 O	Arg17 NH1	2.81	2.78

* Major 2–10–45 interactions.

antiparallel β-sheet. The residues 2–10–45 which form a tight hydrogen-bonded cluster responsible for holding the stem and the arm together are conserved. In variance to crambin which has three disulfide bonds the toxin structures are crosslinked by four disulfide bridges. The comparison of intramolecular side-chain contacts in both toxins is presented in Table 3.

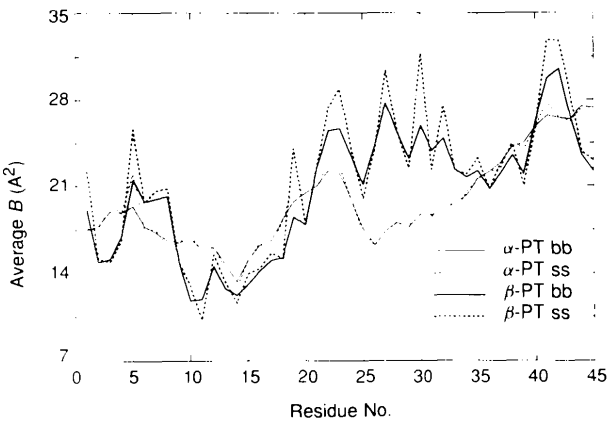

Fig. 5. The comparison of the temperature-factor profiles for α_1-PT and β-PT (heavy dashed and heavy continous lines). Backbone atoms are denoted by bb (in continous lines) while ss denotes side chains (in dashed lines).

Table 4. *Alignment of primary and secondary structures of β-PT with average backbone hydrogen bonds*

Name of secondary-structural element*	Residue span of element	Average φ/ψ (σ φ/ψ) (°)	Average hydrogen-bond distance (Å)
S1	1–4	−114.7(18.6)/ 135.5(15.2)	2.79
T1	5–6	Turn	None
H1	7–18	−63.4(4.5) −39.2(11.7)	2.80
T2	19–21	Helix linker	None
H2	22–28	−69.4(15.8)/ −43.7(9.8)	2.93
T3	29–30	Turn	2.69
S2	31–34	−118.9(15.0)/ 151.2(18.7)	2.79
T4	35–37	β-sheet linker	None
S3	38–39	−110.0/147.0	None
T5	40–44	Type I β-turn	3.21
S4	45	−103.0/172.0	2.75

* Notations used in naming the secondary-structural elements: H = α-helix; S = β-strand; T = reverse turn.

Since the present structure is of higher resolution than that of α_1-PT, an attempt is made to classify different secondary-structural units including the different types of turns. As shown in Table 4 and Fig. 7, the globular fold of β-PT consists of an antiparallel pair of helices (residues 7–18 and 22–28) and two stranded β-sheet (residues 1–4, 31–34 and 45), an extended coil region (residues 38–39) and five turns (residues 5–6, 19–21, 29–30, 35–37 and 40–44). The assignment and average distances of hydrogen bonds formed in different structural units are listed in Table 4. For comparison with crambin refer to Table 4 in Teeter *et al.* (1993).

3.2.1. *Helices.* Two α-helices are found in β-PT (Fig. 7*a*), one with three turns (termed helix *H*1, residues 7–18) and the other with two turns (termed helix *H*2, residues 22–28). The mean torsion angles (φ,ψ) of helices *H*1 and *H*2 are (–63.4, –39.2°) and (–69.4, –43.6°), respectively. Those dihedrals are slightly different from those seen in crambin (–62.1, –39.9°) and (–69.6, –32.0°) indicating a different environment for

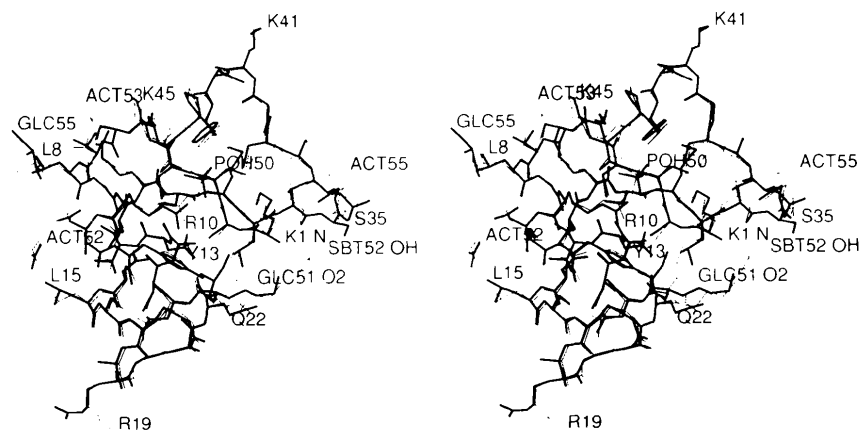

Fig. 6. Superposition of the atomic models of α_1-PT and β-PT showing the difference in conformations of a few of the side chains. α_1-PT is in thin lines and β-PT is in thick lines.

the helices. The *H*1 helix ends with a turn of 3_{10}-helix (Leu15–Ala18).

The backbone hydrogen-bond (O···N) lengths in the helices vary from 2.71 to 3.37 Å with a mean value of 2.94 Å which is close to the expected O—N distances. Asparagine residues are known to introduce distortions to the helices. Although Asn14 did not introduce any major distortions, two other aspargines, 11 and 27, are responsible for small perturbations in the helices. The side-chain N atoms of these aspargines tend to have close encounters with the carbonyl groups of the n_{i+4} residues (Table 2).

It was thought that in crambin Pro19 is responsible for helix termination and the formation of a 3_{10} turn

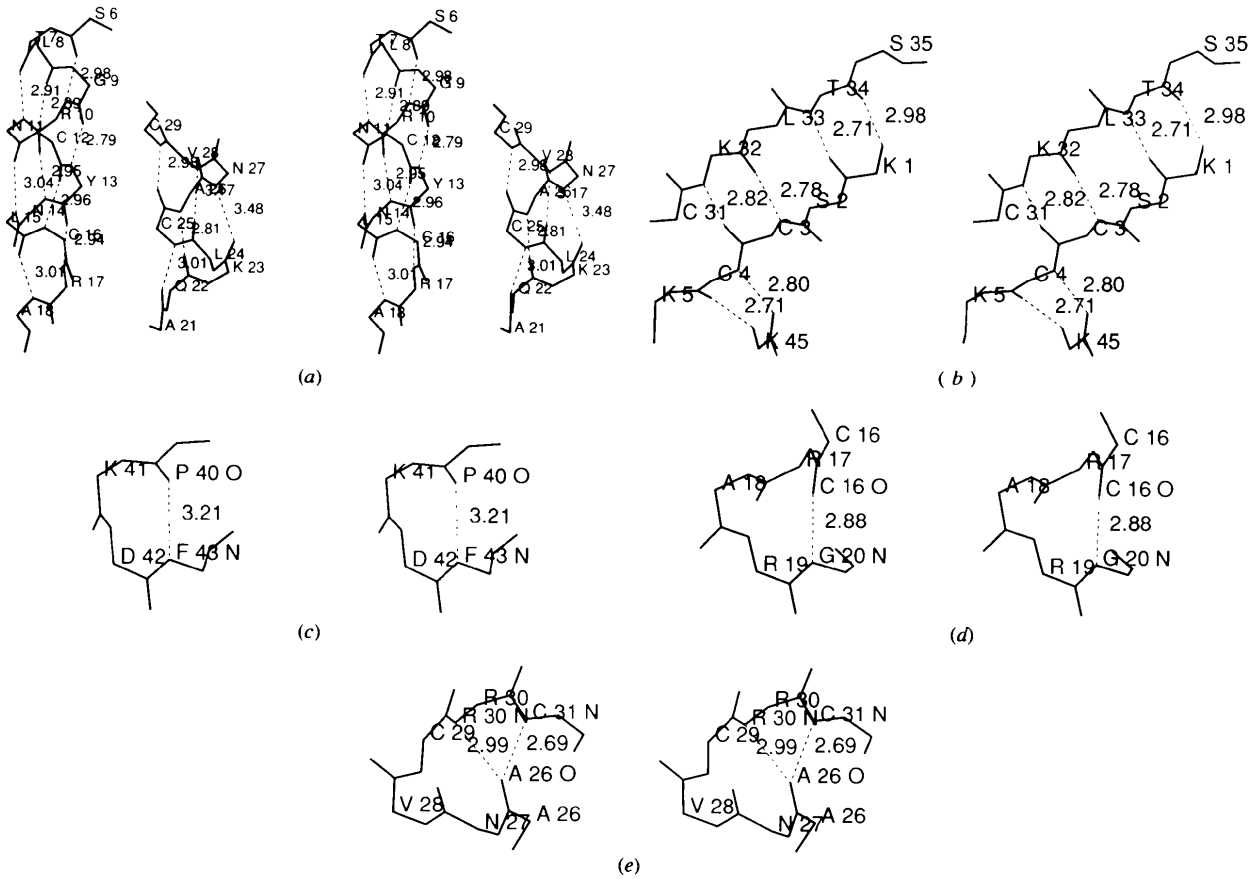

Fig. 7. Backbone atomic models of different secondary structural units in a β-PT. Cα atoms are labeled and hydrogen bonds are shown in broken lines. (*a*) Helices *H*1 (residues 7–18) and *H*2 (residues 21–29). (*b*) β-sheet formed by strands *S*1 (residues 1–4), *S*2 (residues 32–34) and *S*4 (residue 45). (*c*) Turn *T*5 (residues 40–43) in type I β-turn conformation. (*d*) Turn *T*2 between the helices *H*1 and *H*2 showing the α-type twist. (*e*) π-type turn at the C terminus of the helix *H*2 showing $n_i \rightarrow n_{i+5}$ hydrogen bonding between residues 26 and 31.

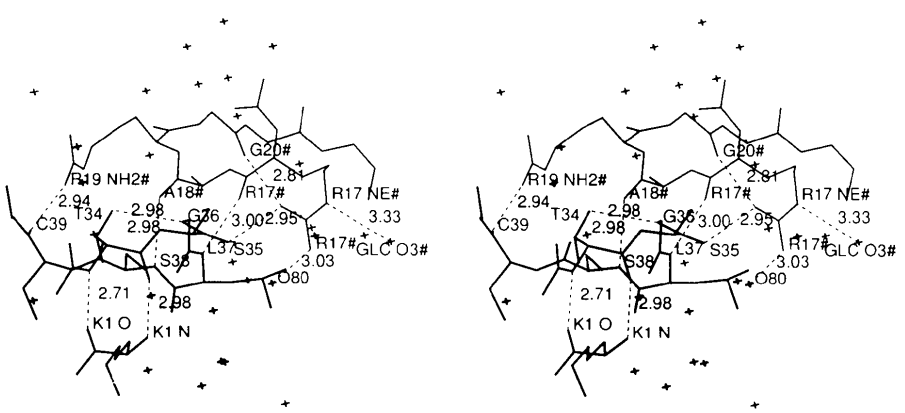

Fig. 8. Stereoview of intermolecular contacts between the symmetry-related molecules involved in interaction *B*. Two backbone hydrogen bonds form a pseudo β-sheet between the end of the *T*4 turn and the *T*2 turn.

towards the end of the helix *H*1. But in both β- and α_1-PT this 3_{10} turn is observed despite the absence of proline at position 19.

3.2.2. *β-strands.* There are four short strands in the structure each containing one to four residues (residues 1–4, 32–34, 38–39 and 46 for the strands *S*1, *S*2, *S*3 and *S*4 respectively). Three of them are hydrogen bonded and form an antiparallel β-sheet (*S*1–*S*2, *S*2–*S*4; Fig. 7*b*) with hydrogen bonds listed in Table 3. The *S*3 strand is not involved in intramolecular sheet formation but is involved in intermolecular contacts (Fig. 8). The average (φ,ψ) torsion angles over all β-strand residues are (–116.5, 145.7°).

3.2.3. *Turns.* There are five turns in the structure of β-PT (residues 5–6, 19–21, 30–31, 35–37, 40–44 for turns *T*1 to *T*5). Turns *T*4 and *T*5 are similar to those of crambin. *T*5 is a classical type I β-turn (see Fig. 7*c*). It has a weak hydrogen bond between the carbonyl group of Pro40 and amide N atom of Phe43 (3.12 Å).

The *T*2 turn between the *H*1 and *H*2 helices is considerably different from that in crambin but very similar to that in α_1-PT. In crambin, due to the presence of Pro at position 19, this turn is a classical type I β-turn. But in β-PT, the deletion of one residue together with the residue change from Pro19 to Arg19 is responsible for the change in conformation of this turn to an α-helical turn ($n_i \rightarrow n_{i+4}$ hydrogen bonding) with the carbonyl O atom of Cys16 bonding to the amide N atom of Gly20 (Fig. 7*d*). The *T*3 turn constitutes another example of a turn architecture where $n_i \rightarrow n_{i+5}$ residues form a hydrogen bond which is reminiscent of the π helix bonding pattern.

3.3. *Crystal packing*

The essential features of the overall crystal packing have been discussed in the previous publication (Teeter *et al.*, 1990) but are repeated here because of key solute reported here mediating these interactions. In brief, there are four kinds of intermolecular interactions, termed *A*–*D*, which help the molecules associate into clusters (Fig. 9*a*). Interaction *B*, because of its hydrophobic nature, forms a hydrophobic dimer whereas interaction *D* forms a polar dimer. Both together result in a tetrameric cluster.

Because of the finding of various solutes in between the interacting surfaces, additional details have been revealed for the polar dimer interaction *D*. More solute-mediated contacts have been found which appear critical not only for the stability of the lattice but also for the lytic activity of the molecules.

3.3.1. *Dimer association.* Two types of dimers can be characterized by looking at the tight contacts at the interaction sites *B* and *D*. The contact *B* could be called a hydrophobic dimer as it is mediated by leucine-ladder type interactions between the first helices of two molecules. The second interaction *D* can be called hydrophilic (it is primarily polar but involves some van der Waals contacts).

Interaction *D* is the strong polar dimer contact between the residues of the first helices of a molecule with the corresponding residues of the twofold symmetry-related molecule. As seen in Table 5, the protein–protein interaction in this dimer is both through intermolecular hydrogen bonds between two aspargines, Asn11 and Asn14 and through van der Waals contact between the CG atoms of symmetry-related Arg10 and CG of Leu15. But a number of other polar and charged residues such as Lys1, Lys45, Arg10, Ser38 and the carboxy terminus are exposed to the interface between the two monomers in this dimer. As a result, several solvent and solute molecules such as acetate, phosphate ion, glycerol and several water molecule are bound here which further strengthen the interactions in this dimer (see below).

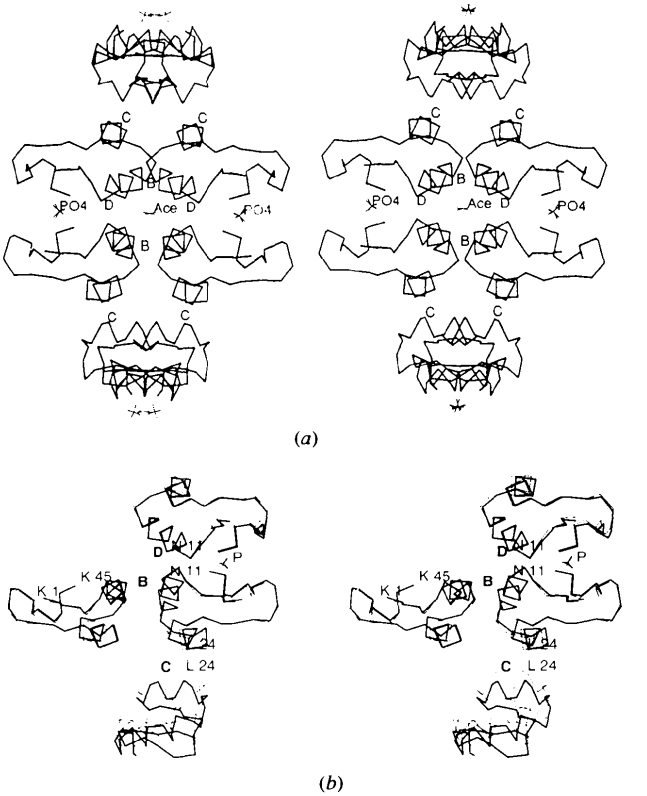

Fig. 9. (*a*) Stereo diagram of intermolecular interactions for α_1-PT viewed down the *b* axis (at $x = \frac{1}{2}$, $y = 0$). A twofold symmetry mate (along the *b* axis) for this 'dimer' shows a hydrophobic interaction of the second helices (*C*) resulting in a 'weak tetramer'. A diagonal twofold at ($x = \frac{1}{2}$, $y = 0$), operating on the *B* dimer, produces the polar-dimer interaction *D*. Association of dimers *B* and *D* is termed as a 'tight tetramer'. The solutes (phosphates and acetates) that bridge the polar dimer tightly are also shown. (*b*) Stereoview of Cα atomic model of α_1-PT (light lines) and that of β-PT (dark lines) showing symmetry-related molecules involved in interactions *C* and *D*. One of the monomers of each purothionin is superimposed. Phosphate ions bound at the *D* interface are also shown. Note the small conformational changes of the backbone and expansion of the β-PT lattice at the *C* interface.

Table 5. *Interactions that stabilize the polar dimer in both α_1- and β-PT*

Atom from a monomer	Atom of a symmetry-related molecule	Distance in β-PT (Å)	Distance in α_1-PT (Å)
Asn11 OD1	Asn14′ ND2	2.80	2.84
Thr7 O	Asn14′ ND2	3.37	3.65
Asn11 ND2	Asn11′ O	3.45	3.90
Asn11 ND2	Acetate	2.73	2.66
Lys1 NZ	Phosphate	Not observed	2.91
Lys45 OT	Water60 (101)*	2.71	3.47
Water60 (101)*	Asn14 ND2	3.10	3.33
Pro44 O	Phosphate	Not observed	3.27
Phosphate	Pro44′ O	Not observed	3.27
Lys1 NZ	Water61′	2.80	Not observed
Water61′	Phosphate	3.00	Not observed
Ser2 OG	Water61′	2.88	Not observed
Ser38 OG	Water100′ (79)*	2.61	3.0
GLC54(180) O1†	Ser2 OG	2.96	3.09
GLC54(180) O2†	Lys45′ NZ	2.94	Not observed
GLC54(180) O2†	Glyn23 OE1	Not observed	2.88
GLC54(180) O3†	Tyr13 OH	3.15	3.36
GLC54(180) O3†	Arg17 NE	3.53	3.41
GLC55 O2	Asn14′ O	2.95	Not observed
ACT52 O1	Asn11 ND2	2.73	3.01
ACT53 O2	Arg30′ NH2	2.84	Not observed
ACT88 O2	Ser35 N	Not observed	2.87
GLC181 O2†	Lys1 N	Not observed	2.84
Sec-But OH	Thr7 OG1	Not observed	3.45
Arg10 CG	Arg10′ CG	3.38	3.62

* Water60 and 100 in β-PT corresponds to water101 and 79 in α_1-PT, respectively.

† Glycerol (GLC) 54 in β-PT corresponds to GLC180 in α_1-PT. Glycerols 54 and 55 are in β-PT while 180 and 181 in α_1-PT.

3.3.2. *Tetramer association.* Various pairs of interactions may lead to higher order associations that may be relevant in solution. The tightest of these are the hydrophobic dimers (*B*) on two different levels, which make tetramer contacts through the polar dimer interaction *D* resulting in a compact tetramer (Fig. 9). This tetramer can also be thought of as a four-helix bundle (see Fig. 9), although the interaction between the helices is not of the conventional type (Cohen & Parry, 1990). The helices here are held by the already mentioned leucine ladders in one direction and with hydrogen bonds between aspargines in the perpendicular direction. This tetramer may be the building block or the seed for crystal growth of α_1- and β-PT.

3.3.3. *Crystal packing modification in β-PT.* Because of high sequence identity, the structures of α_1 and β-purothionins are similar. But the small sequence differences between β-PT and α_1-PT have significant effects on the crystal lattice. Such differences along with their consequences are discussed below.

Just as α_1-PT, β-PT crystallizes in the space group *I*422 and its crystal has a similar layer-like structure having the interactions A, *B*, *C*, *D* and *E* (Rao *et al.*, 1995). There is, however, a 3 Å difference in the *c*-dimension in β-PT crystals compared to α_1-PT. This difference has an important bearing on the packing relationship between molecules. Understanding this relationship in turn may aid in finding the causes of differences between the physical properties for the two purothionin crystals.

The difference in the *c* unit length can be explained in terms of variations in interlayer distances between the two crystals (see Fig. 9*b*). One of the monomers of each α_1- and β-purothionins are superimposed in this figure and corresponding symmetry-related molecules (related by interaction *C* and *D*) are generated. It can be seen from this figure that the monomers related by interaction *C* (β-PT molecules depicted in thick lines and α_1-PT molecules in thin lines) move apart in *c* direction and this movement is about 1.6 Å. The polar dimer *D* is almost identical in β-PT as compared to that in α_1-PT. Since there are two such instances for one unit cell, the net increase or expansion of the cell is about 3 Å in the *c* direction.

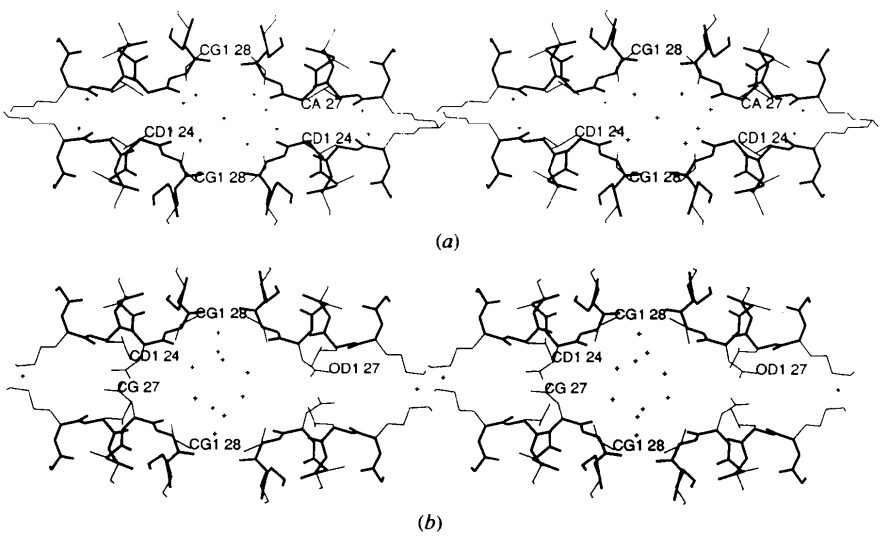

Fig. 10. Stereoviews of atomic model of the weak-tetramer (two *C* dimers related by twofold symmetry along the *c* axis in both α_1-PT and β-PT). Only *H*2 helices are shown. Backbone atoms are shown in thick lines while the side chains are shown in thin lines. Relevant atoms are labeled. (*a*) View for α_1-PT. Note the closeness of Cα of Gly27 and Cδ of Leu24. A single water molecule is packed in between four symmetry-related Val28 residues. (*b*) Similar view for β-PT. Note the expansion in *c* direction, thus making possible the packing of Asn27 side chain at the interface. Moreover, several water molecules are packed between Val28 residues.

Table 6. *Comparison of side-chain conformations between α_1- and β-PT*

	Conformation*									
	β-PT					α_1-PT				
Residue	χ_1	χ_2	χ_3	χ_4	χ_5	χ_1	χ_2	χ_3	χ_4	χ_5
Lys1	t	t	t	+		t	t	t	−	
Arg19	−	−	t	+	t	−	−	−	−	t
Lys23	−	t	t	−		−	−	t	t	
Arg30	−	t	+	+	t	−	t	t	t	t
Lys32	−	t	t	+		t	t	t	t	
Lys41	+	t	t	+		t	t	t	t	

* Abbreviations: t $\simeq 180°$; − $\simeq -60°$; + $\simeq +60°$.

The expansion of the *C* interface region as a result of Gly27→Asn27 change weakens interaction *C* further. This weakened *C* interaction explains several of the observed crystal properties. The β-PT crystals are more sensitive to mechanical strain than those of α_1-PT. They develop cracks along planes perpendicular to the *c* axis. Moreover, the crystals have a tendency to cleave along

The reasons for this cell expansion have their roots in a single residue change at position 27 (Gly to Asn). Fig. 10 illustrates this point. Fig. 10(*a*) shows a view of the weak tetramer in α_1-PT depicting the close contact between four symmetry-related Val28 residues with a single water packed between them. Moreover, there is a van der Waals contact between the side chain of Leu24 and the Cα atom of Gly27 of another molecule which makes interaction *C* with the former. Fig. 10(*b*) shows the corresponding view in β-PT. Here the side chain of Leu24 is in van der Waals contact with the side chain of Asn27 and not with the backbone Cα of this residue. Two monomers making this interaction are pushed apart to accommodate the side chain of Asn27 in between and more waters are added between protein molecules.

these planes and thin sections can easily be peeled off these crystals.

The polar dimer interactions in both the purothionins are listed in Table 5 for comparison. One important change in this dimer for β-PT is related to the formation of four side chain–backbone intermolecular stabilizing hydrogen bonds in addition to the two intermolecular hydrogen bonds between the side chains of Asn11 and Asn14 that exist in α_1-PT. The side chain–backbone hydrogen bonds exist between Asn14 ND2 and Thr7′ O and between Asn11 ND2 and Asn11′ O (see Table 5).

Despite the conformational changes of the side chains (Table 6), the backbone atoms of β-PT generally match well with those of α_1-PT (Fig. 6). The r.m.s. deviation between the positions of the backbone atoms of α_1- and β-purothionins is 0.36 Å whereas a difference of 0.94 Å is observed when all the homologous side chains are also included in the calculation.

There are, however, a few minor differences in the backbone of residues 33–37 of the floppy loop and in residues Arg19 and Gly20 of the turn between the helices. There is about a +20° difference in φ angles of these residues compared to those in α_1-PT. Moreover, the backbone atoms of these residues have an r.m.s. difference in their atomic positions of 0.51 Å compared to 0.36 Å for all the backbone atoms. This change in the backbone contributes to the altered conformation* for Arg19 (−, −, t, +) in β-PT rather than the (−, −, −, −) as seen in α_1-PT. As a result in β-PT, the guanidinium head of this residue is oriented towards the solvent cavity.

3.4. *New solute molecules essential for the lattice formation*

The new features of the structures that were not seen earlier are provided by the solute molecules found in both structures. All of these solute molecules are tightly bound through several contacts, the majority of them being electrostatic as well as polar. The fact that these solutes and solvents, especially phosphate and glycerol, which are located in the lattice even though they were absent in the crystallization medium, may have biological significance. Their presence may reflect the existence of a phospholipid-binding site which is important for the toxic effect exerted on the membrane.

3.4.1. *Phosphate-binding site.* In both α_1- and β-purothionins, there is a specific phosphate-binding site at the *D* interface discussed above. The polar dimer anchored by Asn11 and Asn14 results in a site with relatively high positive electrostatic potential. The site is formed at the center of the polar dimer due to the closeness of two symmetry-related Arg10 and two Lys1 residues and the N terminus (Figs. 2 and 9). In α_1-PT, the phosphate ion binds to symmetry-related pairs of NZ atoms of Lys1. Due to the small conformational changes caused by the different packing in β-PT, the phosphate ion causes a change in Lys1 conformation which makes the direct coordination impossible (see Fig. 6 and Table 5). Phosphate in β-PT is coordinated to two Lys1 through the water molecules.

3.4.2. *Glycerol-binding site.* Both α_1- and β-purothionins have a specific glycerol-binding site at the same location which is close to the phosphate-binding site. Glycerol is bound to the residues that outline the groove between the helical stem and the β-sheet arm (Figs. 2 and 6). In both structures the O3 of the glycerol molecule is bound to the hydroxyl O atom of Tyr13 and the NE of Arg17 whereas O1 is bound to Ser2 OG. There is, however, a difference between them as well. In β-PT, the O2 of glycerol molecule is hydrogen bonded to the symmetry-related Lys45, but in α_1-PT, the glycerol O2 atom interacts with Gln23. Thus, we see that the rearrangement of the unit cell and compaction of the *D* contact causes the glycerol molecule to change a partner in the interaction. The NZ atom of Lys45

* The notations used in this paper for the description of side-chain conformations are t = 180°, + = +60° and − = −60°. These definitions are the same as those used by Ponder & Richards (1987). The corresponding IUPAC convention is t = 180°, g^- = +60° and g^+ = −60°.

is more positively charged and a better donor for a hydrogen bond.

3.4.3. *Acetate-binding site.* Disordered acetate found in both α_1- and β-PTs is located in the four-helical bundle formed by four symmetry-related molecules. The presence of the acetate is reminiscent of the four-helix bundle of cytochrome *B* in which the heme group is found in the middle. Each disordered acetate forms hydrogen bonds to two symmetry-related Asn11 residues protruding toward the center (N Asn11 to O Ace, 2.7 Å). In such a location, it helps to neutralize this extremely positively charged molecule (+9) and contributes to the stability of the lattice.

We may conclude that without those negatively charged solute molecules (phosphate and acetate) placed on the symmetry elements it would be impossible to form the α_1-PT crystals. The intermolecular side-chain interactions which are responsible for the packing with their updated distances are listed in Table 5.

4. Summary

The structure determination of β-PT at higher resolution (1.7 Å) than α_1-PT (2.5 Å) has opened a new vista to understanding more about thionins in general. The initial failures in obtaining high-quality crystals of β-PT and then the difficulties in handling the crystals once they were obtained led us to not only look for crystal-stabilizing factors but also to look into the root causes of these crystal properties. Rerefinement of α_1-PT followed by the parallel refinement of β-PT in the final stages of α_1-PT refinement proved complementary and facilitated locating many critical solute particles in the lattice. The importance of the phosphate and acetate ions in stabilizing both crystals has thus been investigated.

Although the structure of β-PT has overall similarity to that of α_1-PT, there is a key difference between the two in crystal packing. The *c* dimension of the former is larger than that of the latter by 3 Å, and this expansion, originating from a change of residue 27 (Gly→Asn), has been attributed to the altered space between stacking layers of tetrameric molecules. Consequently, some of the side chains have different conformations and the crystals have different properties. The non-homologous amino acids are responsible for the toxins specificity toward different phospholipids (Garcia-Olmedo, Rodriquez-Palenzuela, Hernandez-Lucas, Ponz & Marana, 1989). Thus, the conformational changes might be pertinent to the modulation of biological activity. Modeling may clarify this difference further.

The finding that phosphate ions and glycerol molecules bind to purothionins has led us to believe that it may be relevant to biological activity of the thionins. It is reasonable to assume that those moieties are indicators of the phospholipid-binding site. Experimental support for this hyphothesis comes from Wada, Ozaki, Matsubara & Yoshizumi (1982) and Evans, Wang, Shaw & Vernon (1988). They showed that the toxins lose their toxicity when Tyr13 is iodinated. In our structure the glycerol molecule is bound to this crucial residue. The iodination would disrupt the glycerol and the phospholipid binding thus making the protein impotent towards membranes.

To elucidate the details of these important interactions we have carried out NMR experiments on binding inorganic phosphates and glycerol-3-phosphate and small phospholipid analogs (Markman *et al.*, 1992). Further the NMR three-dimensional structure determination of the α_1-PT–glycerol-3-phosphate complex is in process. The results, which will be presented elsewhere, indicate that this site is indeed the phospholipid binding site. Thus, although preliminary, these results seem to support the crystallographic finding suggesting that the phosphate-binding site is not an artifact of the symmetry of the crystal lattice, but indeed related to the toxicity of these proteins.*

The authors wish to thank the NIH (GM 38114 and GM 40601) for support of this research and Dr B. Jones for the purified proteins. We also thank O. Markman for reading the manuscript and conducting the NMR experiments. Some of the authors also received graduate stipends (UR) or postdoctoral fellowships (UR and BS) from this grant.

* Atomic coordinates have been deposited with the Protein Data Bank, Brookhaven National Laboratory (Reference: 1BHP). Free copies may be obtained through The Managing Editor, International Union of Crystallography, 5 Abbey Square, Chester CH1 2HU, England (Reference: GR0393). At the request of the authors, the atomic coordinates will remain privileged until 15 March 1996.

References

ASHIDA, T., TSUNGOAE, Y., TANAKA, I. & YAMANE, T. (1987). *Acta Cryst.* B**43**, 212–218.

BOHLMAN, H. & APEL, K. (1991). *Ann. Rev. Plant Physiol. Plant Mol. Biol.* **42**, 227–240.

BRÜNGER, A. T. (1992*a*). *X-PLOR, Version* 3.1, *A System for X-ray Crystallography and NMR*. New Haven and London: Yale Univ. Press.

BRÜNGER, A. T. (1992*b*). *Nature (London)*, **355**, 472–475.

CARRASCO, L., VASQUEZ, D., HERNANDEZ-LUCAS, C., CARBONERO, P. & GARCIA-OLMEDO, F. (1981). *Eur. J. Biochem.* **116**, 185–189.

COHEN, C. & PARRY, D. A. D. (1990). *Proteins Struct. Funct. Genet.* **7**, 1–15.

EVANS, J., WANG, Y., SHAW, K.-P. & VERNON, L. P. (1989). *Proc. Natl Acad. Sci.* **86**, 5849–5853.

HERMANS, J. JR & MCQUEEN, J. E. (1974). *Acta Cryst.* A**30**, 730–730.

LUZZATI, V. (1952). *Acta Cryst.* **5**, 802–810.

MARKMAN, O., RAO, U., LEWIS, K. A., HEFFRON, G. J., STEC, B. & TEETER, M. M. (1992). In *New Developments in Lipid–Protein Interaction and Receptor Function*, edited by K. A. WIRTZ & T. A. GOOSTAFSSON. London: Plenum Press.

PONDER, J. W. & RICHARDS, F. M. (1987). *J. Mol. Biol.* **193**, 775–791.

GARCIA-OLMEDO, F., RODRIQUEZ-PALENZUELA, P., HERNANDEZ-LUCAS, C., PONZ, F. & MARANA, C., (1989). *Oxford Surv. Plant Mol. Cell Biol.* **6**, 31–60.

Polygen Corporation (1991). *QUANTA Version* 3.2., *Users Guide*, Polygen Corporation, Waltham, MA, USA.

RAO, U., STEC, B. & TEETER, M. M. (1995). *Acta Cryst.* D**51**, 904–913.

ROE, S. M. & TEETER, M. M. (1993). *J. Mol. Biol.* **229**, 419–427.

SHERIFF, S. (1987). *J. Appl. Chem.* **20**, 55–57.

TEETER, M. M., MA, X.-Q., RAO, U. & WHITLOW, M. (1990). *Proteins Struct. Funct. Genet.* **8**, 118–132.

TEETER, M. M., ROE, S. M. & HEO, N. H. (1993), *J. Mol. Biol.* **230**, 292–311.

WADA, K., OZAKI, Y., MATSUBARA, H. & YOSHIZUMI, H. (1982). *J. Biochem.* **91**, 257–263.